IMPACT OF OLIVINE ON REFRACTORY CORROSION RESISTANCE

Tyler Richards*, Jeffrey Smith, Ronald O'Malley, Todd Sander
Missouri University of Science and Technology, Rolla, MO, USA

ABSTRACT

The corrosion behavior of dry vibratable tundish lining materials was studied. Compositions were batched using periclase and increasing amounts of olivine. A corrosion cup test was employed to react the refractory material with a basic commercial tundish flux. Cathodoluminescence was employed to highlight the migration of silica within the refractory samples, and the chemistry of the resulting phases was determined using energy dispersive spectroscopy. FactSage was used to predict the phases present in the samples and suggest possible reaction mechanisms that would result in the loss of olivine aggregates from tundish lining material.

INTRODUCTION

A tundish is a vital tool in continuous casting of steel. Serving as an intermediate vessel between the ladle and the mold, it allows for a constant flow of steel to be managed without flow interruption during ladle changes. In addition, tundishes give a steel melt time to homogenize thermally and chemically. The lining of a tundish is designed to be quickly changed after each casting sequence. These linings have been applied in a myriad of ways. Some practices have used preformed boards or bricks, while others have used form-in-place methods, such as through a sprayable/gunnable mix. Another installation method that is common today is dry vibratable material. This is a refractory that is supplied as a dry mix, typically with a resin binder, that is fed into the tundish form around a mandrel. This mandrel both vibrates to assist in consolidation of material and heats to cure and polymerize the resin binder.

When selecting a tundish refractory material, consideration must not only be given to molten steel containment but also to the cover flux that the refractory may encounter. In a tundish, a flux is added that melts and floats on the surface of the steel bath. This flux serves three main purposes: minimizing heat loss to the environment, diminishing excess oxygen from ambient air dissolving into the steel, and to aid in the removal of inclusions in the steel. For example, some tundish cover fluxes have been formulated to dissolve the alumina inclusions that form in Al-killed steel[1,2]. Fluxes such as this can be highly basic in nature, containing predominately CaO (when molten) and less than 10 wt% SiO_2. Therefore, a basic refractory material is most suited for the lining. Periclase (MgO) is a commonly employed material for tundish linings. The periclase aggregates in these formulations often consist of smaller MgO crystallites bound together by an interstitial phase such as forsterite (Mg_2SiO_4) or monticellite ($CaMgSiO_4$)[3,4]. In an attempt to improve compatibility with tundish flux, some formulations incorporate other magnesium-containing materials such as olivine ($(Mg,Fe)_2SiO_4$). The addition of olivine tends to decrease the basicity gap between the lining and the flux. However, some of these linings were developed for steel mills that use a less basic or even acidic cover flux[5].

In this work, dry vibratable tundish lining compositions were composed in the lab using varying periclase/olivine ratios. A simple cup corrosion test was employed to

assess compatibility between these formulations and a typical industrial tundish cover flux. The observed interactions were categorized through microscopy and chemical analysis. This is a continuation of previous work by the authors of this paper[6], with particular focus on the effect of olivine on corrosion resistance against basic flux.

PROCEDURE

Refractory compositions were batched using periclase and olivine ratios listed in Table I with a constant 5 wt% phenolic resin as a binder. The typical chemistry of each composition is given in Table II. Cylindrical samples ~30 mm in diameter and 35 mm tall with a 10 mm diameter by 25 mm deep hole were formed directly by uniaxially dry pressing 50 g of material at 3300psi (Figure 1 a). This technique ensured consistent size, location, and depth of the cavity between samples. Cup samples were subsequently treated at 371°C (700°F) for 90 minutes to cure the resin prior to testing.

A commercially available tundish cover flux was selected for use in the experiment. The composition is listed in Table III. To decrease melt time, the flux was calcined at 700°C for 5 hours, then pre-fused at 1450°C, after which it was quenched between two copper plates and ground using a mortar and pestle.

Table I. Composition of refractory samples by aggregate (wt%).

Sample	**1**	**2**	**3**
Periclase	80	60	20
Olivine	20	40	80

Table II. Typical composition of refractory samples by oxide (wt%).

Sample	**MgO**	**SiO_2**	**CaO**	**FeO**	**Al_2O_3**
1	86	9	3	2	0.08
2	80	15	2	3	0.06
3	67	27	1	5	0.02

Table III. Composition of the flux (wt%).

SiO_2	**CaO**	**MgO**	**Al_2O_3**	…
4.4	37.5	15.1	21.6	…

…	**Fe_2O_3**	**Na_2O**	**F**	**TiO_2**	**C**
…	0.6	2.6	4.9	0.5	9.9

Flux was added to the cups before being placed in the furnace. First, flux was packed into each cup, then, a graphite crucible with a hole drilled into the bottom was placed on each cup, providing a mechanism for additional flux introduction. This was done to maximize the amount of flux used in the experiment with the goal of ensuring adequate exposure. In total, 3.25 g of flux was added to each cup. Once placed in the furnace, the temperature was ramped to 1600 °C and held for one hour. After naturally cooling in the furnace, the cups were then sectioned longitudinally, mounted in epoxy, and polished.

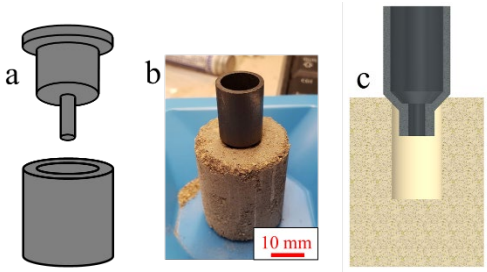

Figure 1. a) Schematic of the custom die press, b) a pressed and cured cup with graphite crucible, and c) a cross section schematic of the cup with crucible.

For each sample cathodoluminescence was first used to survey and identify regions of interest. Cathodoluminescence involves impinging a sample with an electron beam. Depending on the material, this can result in the emission of visible light photons, which can be observed through an optical microscope or recorded with a digital low-light camera.

Cathodoluminescence is a useful compliment to optical microscopy because the colors displayed by the sample are influenced by the chemistry of the phases present, including trace elements. This leads to rapid identification of reaction layers and regions of interest for further analysis[4,6,7]. For chemical analysis, a Tescan Vega-3 scanning electron microscope with a backscattered electron detector and Bruker X-Flash EDS detector was used.

FactSage is a useful tool for thermodynamic calculations. Multiple authors have found ways to use FactSage to predict corrosion behavior in refractories via minimization of Gibb's free energy for refractory/slag systems[8-10]. There are different philosophies regarding how such calculations are formulated. For corrosion of refractory by slag, it is useful to perform an iterative calculation, with each successive calculation fed with the slag product of the previous calculation. This technique helps account for the dynamic slag chemistry during refractory dissolution, and can help determine what phases may precipitate or become otherwise stable as the slag reaches saturation. In this work, such a model is adapted from Luz *et al.*[10], who studied the corrosion of spinel castables by ladle slag. Calculations were performed using the Equilib module of FactSage 8.0 to determine the equilibrium phases of 100 g of refractory and 100 g of flux separately at 1600 °C. All equilibrium phases of the refractory calculation were saved as a stream, and the slag phase of the flux calculation was saved as another. After this "initialization" step, each stream was reacted. The slag phase was again saved and the calculation was repeated, using the new slag in place of the old. This continued until the slag was fully saturated and the solid phases matched the original refractory equilibrium phases. Figure 2 illustrates this as a schematic. The FactPS and FToxid databases were used for these calculations, and a macro was written to automate the process.

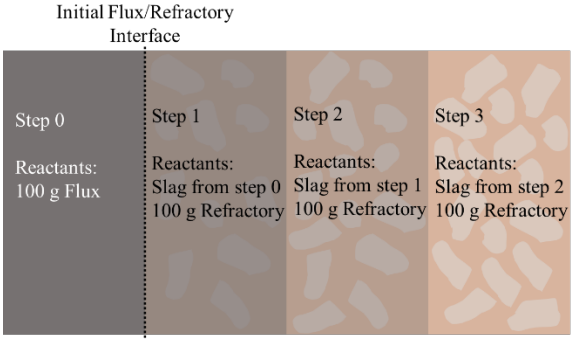

Figure 2. Schematic of the FactSage Model. The mass of flux used for each step is equal to the final slag weight from the previous step.

RESULTS AND DISCUSSION

The results of the FactSage calculations are summarized in Figures 3 and 4. For each refractory composition, olivine is not an equilibrium phase when first reacted with the flux. With each iteration, the amount of flux increased (as the flux stream combines with the slag phase self-generated by the refractory and what formed during the reaction). As it proceeds, the flux accommodates more silica until a solubility limit between 35 and 40 wt% is reached. While all three samples do reach similar levels of saturation, the rate at which this equilibrium is reached may differ. In this regard, as the original olivine content increased, fewer steps were required to reach saturation. At this point, olivine is shown to survive the reaction. On the other hand, while MgO is predicted to be more resistant to corrosion, it does form a solid solution, primarily with ~2-10 wt% FeO (FeO concentration increased with increasing olivine content). The amount of MgO solid solution is higher in the first reaction step than it is in the initialized refractory stream. The resistance of MgO to flux attack can be attributed to the fact that the flux is already saturated with MgO.

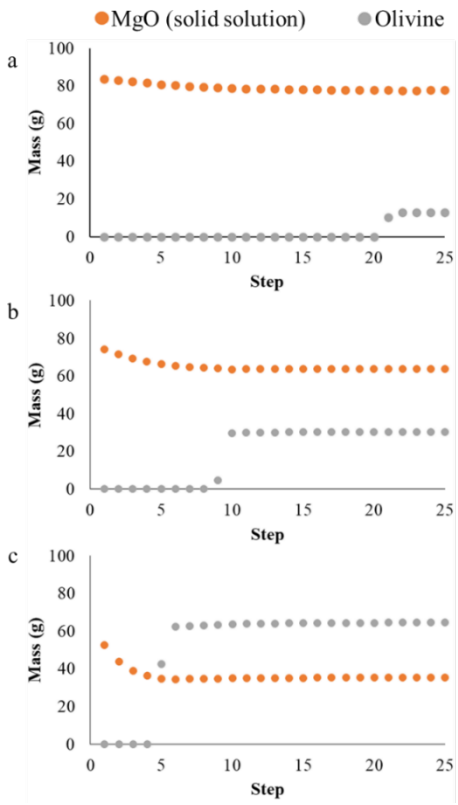

Figure 3. Equilibrium amounts for the solid components of each refractory after reacting with flux (initial total refractory mass: 100g). a) 20 wt% olivine, b) 40 wt% olivine, c) 80 wt% olivine. Each step is an additional iteration of the reaction as illustrated in Figure 2.

The calculated equilibrium of the flux chemistry by itself did in fact result in the precipitation of MgO solid solution (though only the liquid slag phase was used in the flux/refractory reaction). As the flux picked up SiO_2, the amount of MgO solid solution decreased slightly. This indicates an increase in the solubility of MgO in flux, as illustrated in figure 4. No intermediate phases were predicted to form at any stage in the calculation, suggesting dissolution of silicate phases by flux is the prime corrosion mechanism. Cathodoluminescence imagery of the cups are shown in Figure 5. Two main layers are revealed. The inner layer shows a dark purple color throughout. The outer layer displays more intense color (predominately

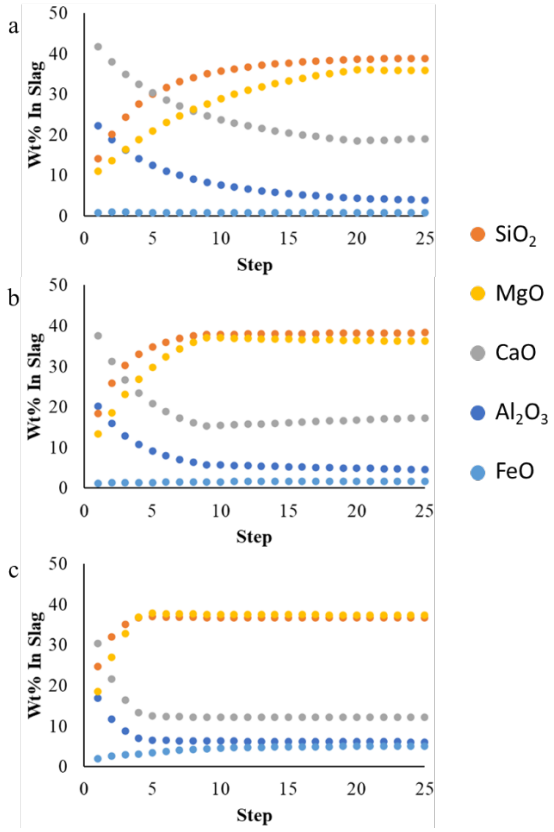

Figure 4. Concentration of major slag components after each iteration. a) 20 wt% olivine, b) 40 wt% olivine, c) 80 wt% olivine.

orange, with yellow and dark purple) indicating the presence of multiple phases.

The depth of the inner layer in cathodoluminescence suggests that the flux penetrated further into the refractory than what might otherwise be apparent optically. The distinct colors between the inner and out layer aid in identifying the physical extent of the reaction.

Scanning electron microscopy and energy dispersive spectroscopy are used to determine the chemistry of the phases present. Figure 6 shows a backscattered electron image of the inner layer of the 20 wt% olivine sample. While cathodoluminescence only displayed one color in the inner layer, multiple phases are present. EDS indicates that the aggregates are MgO, whereas the "matrix" phase consists of a mixture of oxides (see Figure 7). No olivine

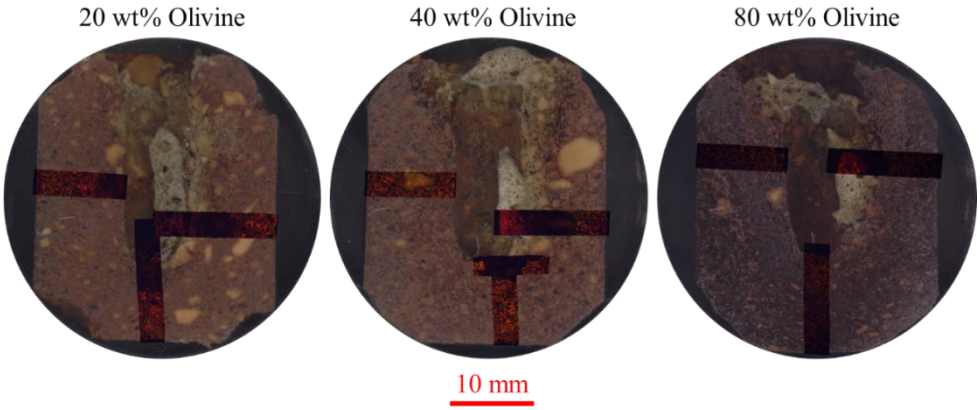

Figure 5. Cathodoluminescence imagery of the three cup samples.

aggregates are detected in this region.

Figure 8 shows a backscattered electron image of the outer layer of the 20 wt% olivine sample. In this case, the periclase aggregates contain their original secondary phase ($CaMgSiO_4$) and olivine aggregates are observed.

The inner layer of the 40 wt% olivine sample is shown in Figure 9. Like the previous sample, the inner layer consists of MgO crystallites in a matrix of other oxides. Figure 9 also shows the outer layer of the 40 wt% olivine sample, where both periclase and olivine aggregates are present. Overall, consistent behavior is seen between samples.

The inner and outer layers of the 80 wt% sample are shown in Figure 10. Here, it becomes especially difficult to distinguish the inner layer from the flux itself. It becomes apparent from these observations as well as from the optical imagery that this sample experienced the most damage to its structure from flux corrosion, as the olivine that made up a significant portion of its structure was fully depleted and replaced by slag. Due to inconsistent wetting of each sample by the flux, penetration depth will not be a useful metric for comparisons.

Cathodoluminescence indicates a relatively abrupt transition between layers. EDS maps taken at a transition between the inner and outer layers of each sample, shown in Figure 11, indicate a drop in Si corresponding to an increase in Al resulting from interaction with flux. This is in agreement with the FactSage model, which predicted total removal of olivine by flux until saturation.

Each sample has a bead of flux remaining in the cavity. The flux shows two phases: a solid phase and a liquid phase. The chemistries of these phases are compared to the matrix phase found in the inner layer of each sample in Table IV. In each sample, the flux liquid phase has a chemistry congruent with the matrix phase within the infiltrated layer. Additionally, the chemistry is similar across samples despite the differences in original refractory composition. The solid phase is excess magnesia in the saturated flux, as predicted in FactSage.

Certain discrepancies exist between the FactSage calculations and experimental observations. however, these discrepancies give insight into the mechanisms behind the observed behavior. FactSage predicted an increase in silica within the flux, but Table IV indicates consistently low silica content throughout in the flux and infiltrated refractory. For this to occur, the silica must be removed from the system in some way. If any residual carbon is left over from the resin binder, FactSage predicts that SiO_2 could be reduced to SiO vapor under the following reaction.

$$SiO_{2(s)} + C_{(s)} = SiO_{(g)} + CO_{(g)}$$

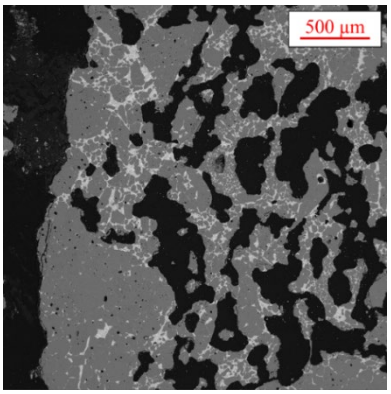

Figure 6. Backscattered electron image of the inner surface of the 20 wt% olivine sample.

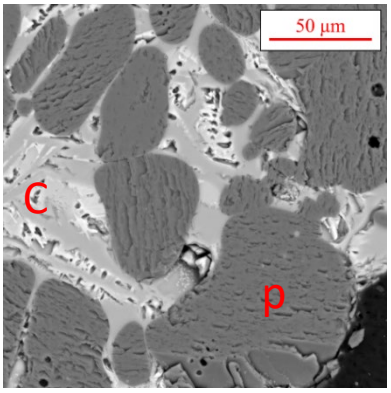

Figure 7. A high-magnification image of an area within Figure 6. The letter "c" denotes a CaO-rich matrix phase. Bright regions in the matrix correspond to relatively higher Ca content. The letter "p" denotes MgO crystallites from the periclase aggregates.

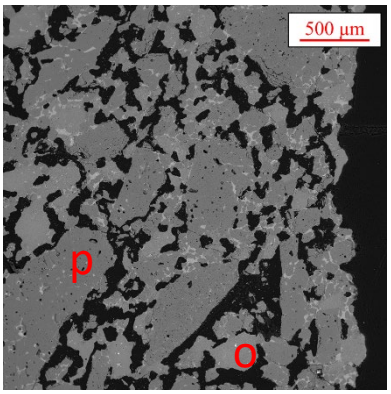

Figure 8. A backscattered electron image of the outer wall of the 20 wt% olivine sample. "p" – periclase; "o" – olivine.

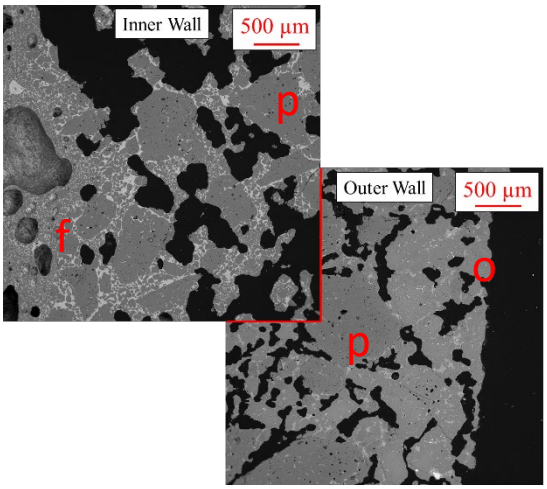

Figure 9. Backscattered electron imagery of the inner and outer walls of the 40 wt% olivine sample. "p" – periclase; "o" – olivine; "f" – flux.

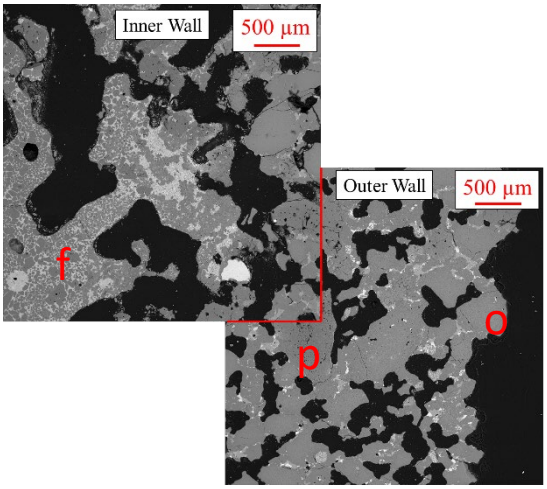

Figure 10. Backscattered electron imagery of the inner and outer walls of the 80 wt% olivine sample. "p" – periclase; "o" – olivine; "f" – flux bead.

For this to occur, the partial pressure of O_2 would need to be below 10^{-5} atm. If the removed silica-rich phases are not kept in the infiltrating flux, then the flux will not reach saturation and the observed corrosion behavior may continue unabated.

It should be noted that using FactSage to model corrosion does not take kinetic factors into consideration. While the refractory compositions may be compared in terms of number of steps to reach flux

saturation, these steps do not have an actual unit of time associated with them.

While FactSage did not predict additional phases forming from the reaction,

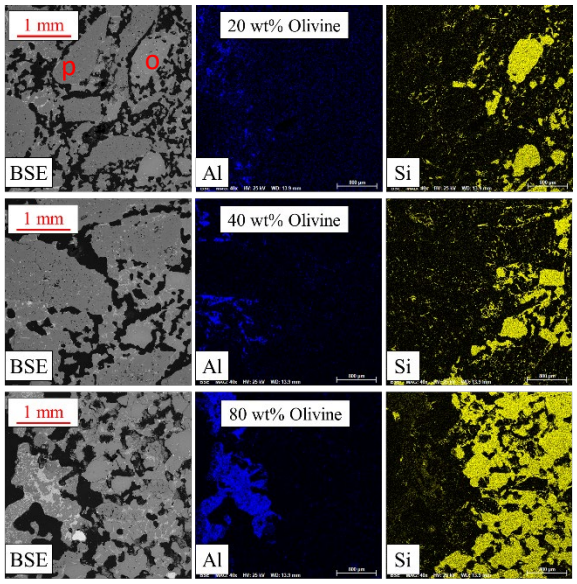

Figure 11. Aluminum and silicon EDS maps of the interface between the two regions identified by cathodoluminescence (Figure 4). "p" – periclase; "o" – olivine.

Table IV. Standardless EDS quantification of selected phases within each sample.

Infiltrated Matrix ("c" in Figure 7)						
Sample	**O**	**Mg**	**Al**	**Si**	**Ca**	**Fe**
1	16	4	27	2	49	2
2	15	1	22	3	53	5
3	10	1	16	3	47	6
Flux, Liquid Component						
Sample	**O**	**Mg**	**Al**	**Si**	**Ca**	**Fe**
1	14	1	22	2	59	1
2	15	3	22	2	56	2
3	13	--	26	2	59	--
Flux, Solid Component						
Sample	**O**	**Mg**	**Al**	**Si**	**Ca**	**Fe**
1	21	79	--	--	--	--
2	21	79	--	--	--	--
3	19	81	--	--	--	--

some spinel did form as the alumina-rich slag contacted the magnesia particles in the refractory. Figure 12 gives an example of this spinel formation. Spinel has high refractoriness and may be ideal for some applications but is also a concern for steel plants as the angular grains can have a negative impact on steel quality if spinel is to spall off the refractory and become a steel inclusion. This behavior was observed in the 40 and 80 wt% samples, but not in the 20 wt% sample.

Both the FactSage calculations and the experiment indicate magnesia was more resistant to corrosion from the flux. The magnesia crystallites also contain some amount of iron oxide. Pal *et al.*[11] note that iron oxide from olivine may diffuse into MgO to form magnesiowüstite, which can decrease the melting temperature of the refractory. Similar behavior has been observed by the current authors[12]. This, in addition to the interaction between flux and the secondary phases binding the MgO crystallites together, contribute to the overall degradation of the refractory from flux attack. This behavior has been observed with low-basicity fluxes as well, wherein the dissolution of silicate phases into the flux led to a decrease in flux viscosity, aiding in further penetration into the refractory[13].

CONCLUSIONS

The quick dissolution of olivine/SiO_2-rich phases into flux was identified as the main corrosion mechanism for three tundish lining refractory compositions. The flux was never saturated by SiO_2, indicating that corrosion could have occurred for much longer than tested, possibly indefinitely. The periclase aggregates exhibited better corrosion resistance, however the risk remains of flux interacting with the secondary phases within the aggregates, leading to a compromise of the refractory's structure.

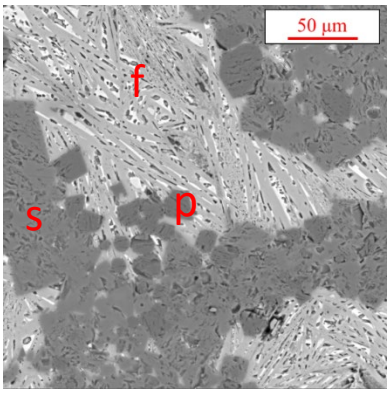

Figure 12. Spinel formations found near the inner wall of the 80 wt% olivine sample (see Figure 10). “s” – spinel; “p” – MgO; “f” – flux.

REFERENCES

1. L. Holappa, M. Kekkonen, S. Louhenkilpi, R. Hagemann, C. Schröder, and P. Scheller, “Active Tundish Slag.” *Steel Research International* 84 [7] 638-648 (2013)

2. M. Kekkonen, D. Leuverink, and L. Holappa, “Improving Cleanliness of 16MnCrS5 Case Hardening Steels by Optimized Active Tundish Flux.” *Steel Research International* 88 [7] 1600364 (2017)

3. M. C. Mantovani, L. R. Moraes Jr, R. Leandro da Silva, E. F. Cabral, E. A. Possente, C. A. Barbosa, and B. P. Ramos, “Interactions between molten steel and different kinds of MgO based tundish linings.” *Ironmaking & Steelmaking* 40 [5] 319-325 (2013)

4. T.M. Richards, R.J. O’Malley, J.D. Smith, and T.P. Sander, “Interactions between Dry Vibratable Tundish Linings and Steel Melts.” *Proceedings of AISTech 2020*

5. M. Kalantar, B. M. Moshtaghioun, and A. Monshi, “Developing Two New Tundish Plasters and Comparing with the Magnesia Plaster Used in Continuous Casting of Steel.” *Journal of Materials Engineering and Performance* 19 [2] 237-245 (2010)

6. T.M. Richards, R.J. O’Malley, J.D. Smith, and T.P. Sander, “Interactions between Molten Tundish Slags and Periclase/Periclase-Olivine Tundish Linings.” *ACerS Refractory Ceramics Division Symposium on Refractories*, St. Louis, Missouri, March 2021

7. M. Karakus and R. Moore, “Cathodoluminescence (CL) Microscopy Application to Refractories and Slags.” *Journal of Minerals and Materials Characterization and Engineering* 1 [1] 11-29 (2002)

8. J. Berjonneau, P. Pringent, and J. Poirier, “The development of a thermodynamic model for Al_2O_3-MgO refractory castable corrosion by secondary metallurgy steel slags.” *Ceramics International* 35 [2] 623–635 (2009)

9. C. Wagner, C. Wenzl, D. Gregurek, D. Kreuzer, S. Luidold, and H. Schnideritsch, “Thermodynamic and Experimental Investigations of High-Temperature Refractory Corrosion by Molten Slags.” *Metallurgical and Materials Transactions B* 48 [1] 119-131 (2017)

10. A.P. Luz, A.G. Tomba Martinez, M.A.L. Braulio, and V.C. Pandolfelli, “Thermodynamic evaluation of spinel containing refractory castables corrosion by secondary metallurgy slag.” *Ceramics International* 37 [4] 1191-1201 (2011)

11. A.R. Pal, S. Bharati, S. Bose, S.K. Choudhury, G.C. Das, and P.G. Pal, “Effect of component variation in CaO-SiO_2-MgO-Al_2O_3 slags on controlling corrosion of olivine based disposable tundish lining material.” *Ironmaking and Steelmaking*, 40 [7] 515-520 (2013)

12. T.M. Richards, R.J. O’Malley, J.D. Smith, and T.P. Sander, “Corrosion Behavior of Tundish Refractories by Molten Steel and Tundish Flux.” *Proceedings of AISTech 2021*

13. A.R. Pal, S. Bharati, N.V.S. Krishna, G.C. Das, and P.G. Pal, “Study of penetration and corrosion of olivine-periclase and periclase based tundish DVMs by molten slag.” *Ironmaking and Steelmaking*, 38 [8] 602-607 (2011)